ACS chemical biology

Articles

pubs.acs.org/acschemicalbiology

Rational Design of Bioactive, Modularly Assembled Aminoglycosides Targeting the RNA that Causes Myotonic Dystrophy Type 1

Jessica L. Childs-Disney,[†] Raman Parkesh,[†] Masayuki Nakamori,[‡] Charles A. Thornton,[‡] and Matthew D. Disney*[,†]

[†]Department of Chemistry, Scripps Florida, 130 Scripps Way, Jupiter, Florida 33458, United States

[‡]Department of Neurology, University of Rochester, Rochester, New York 14642, United States

Supporting Information

ABSTRACT: Myotonic dystrophy type 1 (DM1) is caused when an expanded r(CUG) repeat (r(CUG)^{exp}) binds the RNA splicing regulator muscleblind-like 1 protein (MBNL1) as well as other proteins. Previously, we reported that modularly assembled small molecules displaying a 6′-*N*-5-hexynoate kanamycin A RNA-binding module (**K**) on a peptoid backbone potently inhibit the binding of MBNL1 to r(CUG)^{exp}. However, these parent compounds are not appreciably active in cell-based models of DM1. The lack of potency was traced to suboptimal cellular permeability and localization. To improve these properties, second-generation compounds that are conjugated to a D-Arg$_9$ molecular transporter were synthesized. These modified compounds enter cells in higher concentrations than the parent compounds and are efficacious in cell-based DM1 model systems at low micromolar concentrations. In particular, they improve three defects that are the hallmarks of DM1: a translational defect due to nuclear retention of transcripts containing r(CUG)^{exp}; pre-mRNA splicing defects due to inactivation of MBNL1; and the formation of nuclear foci. The best compound in cell-based studies was tested in a mouse model of DM1. Modest improvement of pre-mRNA splicing defects was observed. These studies suggest that a modular assembly approach can afford bioactive compounds that target RNA.

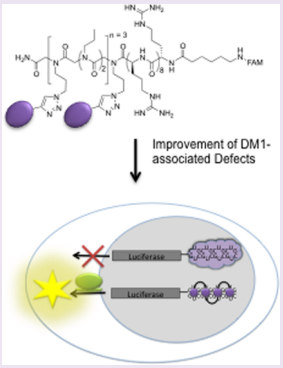

Potential RNA drug targets are plentiful in the transcriptome; however, only the bacterial rRNA, and hence the ribosome, are tried and true targets for small molecules.[1] Ideally, both coding and noncoding RNAs that have important biological functions could be targeted with small molecules.[2] There are significant challenges for the development of small molecules that modulate RNA function, either by screening or rational design. These issues are mainly centered on the identification of selective small molecule ligands that target specific RNAs and parallel efforts to identify the RNA motifs that selectively bind small molecule ligands.[3]

The current state of the art in developing compounds that target RNA is the use of antisense nucleic acids or interfering RNAs.[4−6] Although both of these strategies are powerful, oligonucleotide-based therapeutics can have undesirable properties such as nonspecific stimulation of the immune system and off-target effects.[7,8] In addition, the compounds have poor cellular permeability and are more expensive to manufacture than small molecules. The advantage of oligonucleotides is their unparalleled simplicity of design based on base-pairing rules.

In an effort to develop methods to target RNA with small molecules, our group has developed a program to define a database of RNA motif−ligand interactions by using multidimensional combinatorial screening.[9−12] In this approach, a library of small molecules is probed for binding to a library of discrete RNA motifs that are commonly found in the repertoire human RNA structures (hairpins or internal loops, for example). By selecting RNA motif−ligand binding partners, the optimal RNA motifs that bind small molecules are defined and deposited into the database. This database can be mined against transcriptomic data and secondary structure predictions to determine if a particular RNA has ligand-targetable motifs. The small molecules that bind to these motifs serve as lead compounds to target the RNA of interest.[13−16]

In previous investigations, it was determined that 6′-*N*-5-hexynoate kanamycin A (**K**), binds a 2 × 2 nucleotide pyrimidine-rich internal loop that is present in the RNA that causes myotonic dystrophy type 2 (DM2).[9,12,13] DM2 is caused by an expanded r(CCUG) repeat in intron 1 of the zinc finger 9 protein (*ZNF*9). The expanded repeat folds into a hairpin with an array of 5′CCUG/3′GUCC motifs. These loops serve as a high affinity-binding site for muscleblind-like 1 (MBNL1) protein, a regulator of pre-mRNA splicing.[17] DM2 is associated with the inactivation of MBNL1, which leads to pre-mRNA splicing defects.[18,19] By using the information that **K** binds to RNA motifs like those present multiple times in r(CCUG)^{exp}, a potent *in vitro* inhibitor of the r(CCUG)^{exp}−MBNL1 interaction was designed. Specifically, the optimal multivalent compound displays the **K** module with the same periodicity as the array of 5′CCUG/3′GUCC motifs present in r(CCUG)^{exp}.[13]

Received: April 4, 2012
Accepted: September 18, 2012
Published: November 7, 2012

During the course of studies to understand the RNA targets of 6′-*N*-5-hexynoate kanamycin A, we determined that a suboptimal motif for ligand binding is 5′CUG/3′GUC, the motif that is highly reiterated in the expanded r(CUG) repeat (r(CUG)^{exp}) that causes myotonic dystrophy type 1 (DM1). DM1 and DM2 share a similar molecular basis of disease as both expanded repeats bind and inactivate MBNL1. The r(CUG) expansion is also located in a noncoding sequence, the 3′ untranslated region (UTR) of the dystrophia myotonica protein kinase (*DMPK*) mRNA.[20,21]

It was hypothesized that the optimal distance between **K** modules would be shorter for the DM1 RNA than the DM2 RNA due to the smaller size of the internal loop (Figure 1).

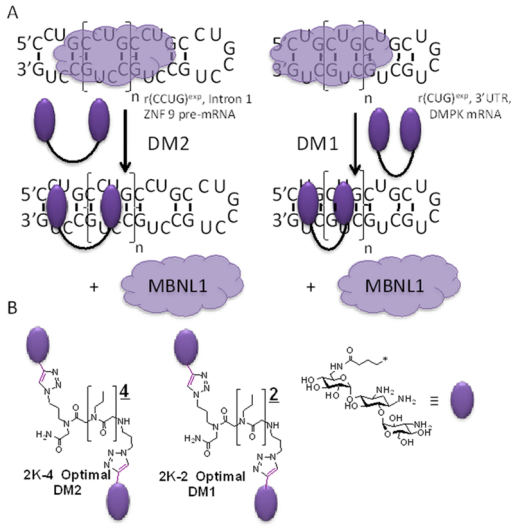

Figure 1. Disease mechanism for DM1 and DM2 and the strategy employed to design modularly assembled small molecules that target the RNAs that cause disease. (A) The secondary structures of r(CCUG)^{exp} and r(CUG)^{exp}, the causative agents of DM2 and DM1, respectively. The expansions bind MBNL1 protein and cause pre-mRNA splicing defects. By using modularly assembled small molecules, the repeats can be effectively targeted to inhibit or displace MBNL1. (B) The structures of the optimal modularly assembled compounds that target DM2- and DM1-causing RNAs by using a 6′-acylated kanamycin A derivative as the RNA-binding module. Previous studies have shown that binding affinity and selectivity can be controlled such that the compounds are specific for DM1 or DM2 RNAs by altering the spacing between the RNA-binding modules.[15] **2K-2** is selective for DM1, while **2K-4** is selective for DM2.

Indeed, by decreasing the distance between **K** modules, a modularly assembled compound that was selective for r(CUG) repeats and potently inhibitory for the r(CUG)^{exp}–MBNL1 interaction *in vitro* was identified.[15] These studies established that both the nature of the RNA-binding module and the spacing between modules are independent determinants of RNA-binding properties of modularly assembled ligands.

In this report, we disclose that second generation modularly assembled compounds that target r(CUG)^{exp} are effective in cell culture and animal models of DM1. These compounds were engineered for enhanced cellular permeability and nuclear localization via conjugation to a D-Arg$_9$ (**DR$_9$**) molecular transporter.[22−25] Specifically, the designer compounds improve pre-mRNA splicing defects in cell culture and animal models, improve translational defects in a cell-based model system, and disrupt the formation of nuclear foci.

RESULTS AND DISCUSSION

We previously reported that modularly assembled small molecules displaying 6′-*N*-5-hexynoate kanamycin A (**K**) inhibit the formation of the r(CUG)^{exp}–MBNL1 complex *in vitro*.[13,15,16] The optimal compounds consist of a peptoid backbone in which the **K** ligand modules are separated by two propylamine spacers. The nomenclature for these structures is **nK-2**, where **n** is the number of RNA-binding modules displayed on a single chain (or valency), **K** indicates the RNA-binding module (a conjugated version of 6′-*N*-5-hexynoate kanamycin A), and the number after the dash indicates the number of propylamine spacers between **K** modules. The structures of these and related control compounds are shown in Figure 2.

Bioactivity of nK-2 Compounds in DM1 Cell-Based Model Systems. The presence of r(CUG)^{exp} causes various defects *in vivo*, including (i) dysregulation of pre-mRNA splicing controlled by MBNL1;[19,26] (ii) nuclear retention and hence decreased translation of r(CUG)^{exp}-containing transcripts;[27,28] and (iii) formation of nuclear foci, which consist of r(CUG)^{exp}–protein aggregates.[29,30]

Two cell-based models were used to determine if the optimal compound from *in vitro* studies, **4K-2**, could improve DM1-associated defects. These assays were completed as described previously.[31] First, the effect of **4K-2** on pre-mRNA splicing was assayed in HeLa cells.[32] Briefly, cells were cotransfected with a DM mini-gene that expresses 960 interrupted r(CUG) repeats and a cardiac troponin T (cTNT) pre-mRNA mini-gene.[31,32] After transfection, the cells were treated with compound in growth medium. cTNT alternative splicing (Figure 3) was then analyzed by RT-PCR and denaturing gel electrophoresis as previously described.[31]

The second model system mimics the *DMPK* translation defect (Figure 4). The C2C12 cell line was stably transfected with the firefly luciferase gene in which d(CTG)$_{800}$ was placed in the 3′UTR.[31] Expression of luciferase is low in this cell line due to the binding of r(CUG)$_{800}$ to MBNL1 and other proteins, resulting in nuclear retention of the luciferase mRNA. If a compound is efficacious, then an increase in luciferase activity in cell lysates is observed.

In both model systems, **4K-2** was not active or only very slightly active at 10 μM (Figure 3). Previous studies of the cellular permeability of **2K-2** and **4K-2** showed that, although the compounds are cell permeable, they localize mainly to the perinuclear region.[13,15,16,33] We hypothesized that, if the cellular permeability and nuclear localization of the compounds could be improved, then the compounds might be efficacious.

Cellular Permeability of nK-2-DR$_9$ Compounds. To develop compounds with increased cellular permeability and nuclear localization, the molecular transporter D-Arg$_9$ (**DR$_9$**)[23,24] was conjugated onto **4K-2** to yield **4K-2-DR$_9$** (Figure 2). Previous studies have shown that multiple guanidinium units facilitate cellular uptake of cargo ranging from small molecules to peptides and proteins.[23,34] Furthermore, mechanistic studies have shown that polyarginines enter mammalian cells through various pathways that include binding to cell surface heparin sulfate and endocytotic uptake.[35] Since many cell and tissue types present heparin sulfate,[36] we envisioned that **DR$_9$** conjugation could engender compounds with the ability to more efficiently enter a variety of cell lines and mouse tissues.

dx.doi.org/10.1021/cb3001606 | *ACS Chem. Biol.* 2012, 7, 1984–1993

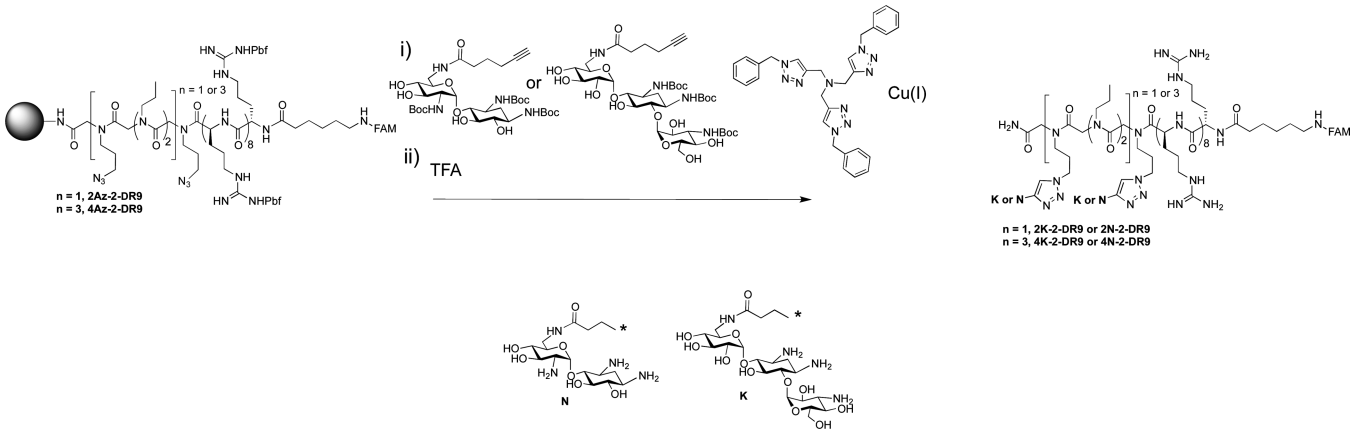

Figure 2. Synthetic scheme used to provide modularly assembled small molecules that target r(CUG)^{exp}. The modularly assembled small molecules were synthesized to contain a D-Arg$_9$ tag to facilitate cellular permeability. Bioactive peptoids contain **K** modules, while control peptoids that have no biological activity contain **N** modules.

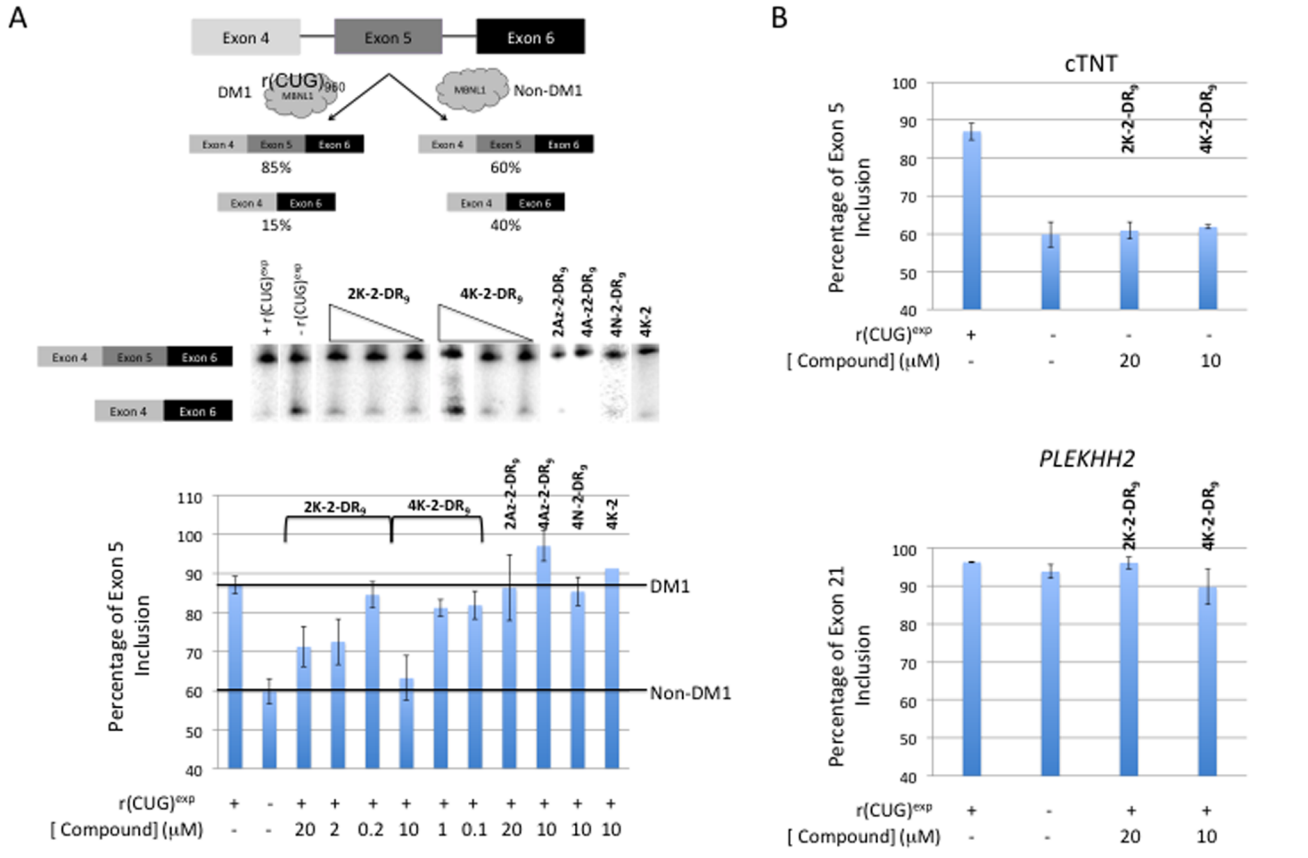

Figure 3. Assessing the bioactivity of modularly assembled small molecules targeting r(CUG)^{exp} in a pre-mRNA splicing defect assay. (A) Top, a schematic of the cTNT mini-gene that was used in this assay. Middle, representative gel autoradiogram assaying improvement of cTNT pre-mRNA splicing when a cellular model system of DM1 is treated with various compounds. Concentrations of compounds correspond to the plot shown below. Bottom, plot of the data for cTNT mini-gene splicing in the presence and absence of modularly assembled compounds. **4K-2-DR$_9$** restores pre-mRNA splicing patterns to levels observed in the absence of r(CUG)^{exp} when cells are treated with 10 μM compound. Modest improvement in splicing defects is observed when cells are treated with lower concentrations of **4K-2-DR$_9$** or with **2K-2-DR$_9$**. (B) Top, **2K-2-DR$_9$** and **4K-2-DR$_9$** do not affect the splicing of the cTNT mini-gene in the absence of r(CUG)^{exp}. Bottom, **2K-2-DR$_9$** and **4K-2-DR$_9$** do not affect the splicing of the *PLEKHH2* mini-gene in the presence or absence of r(CUG)^{exp}. The alternative splicing of *PLEKHH2* is not regulated by MBNL1.

To study if the **nK-2-DR$_9$** compounds have enhanced cellular uptake relative to the parent molecules, flow cytometry experiments were complete using the HeLa cell line as it was also used to assay pre-mRNA splicing defects. Compounds were added in growth medium to the cells and incubated for 1.5 h. The cells were trypsinized from the surface and stained with propidium iodide (detects dead or damaged cells with compromised cell membranes). Since the compounds are labeled with fluorescein, it was used to quantify cellular permeability. Compound **4K-2** was only taken up by ca. 1% of the cells in these conditions, while **4K-2-DR$_9$** was taken up by 13-fold higher number of cells. Two related compounds were

dx.doi.org/10.1021/cb3001606 | *ACS Chem. Biol.* 2012, 7, 1984−1993

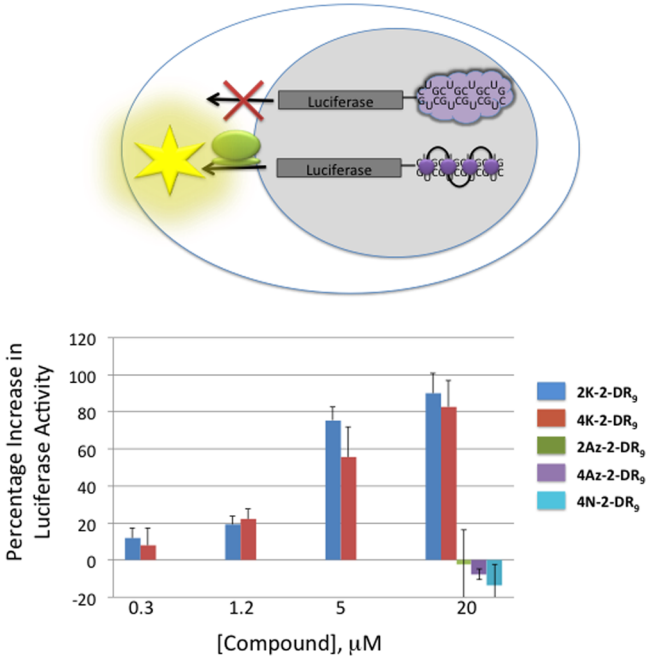

Figure 4. Assessing the bioactivity of modularly assembled small molecules targeting r(CUG)^{exp} in a translational assay. Top, a schematic of the translational assay used to assess the effect of compounds on the DM1 translation defect. Bottom, **2K-2-DR$_9$** and **4K-2-DR$_9$** improve the DM1 translation defect as determined by an increase in luciferase activity. Please note that untreated cells have a percentage increase of luciferase activity value of 0.

also studied, **4N-2-DR$_9$** and **4Az-2-DR$_9$** where **N** indicates the conjugation of 6′-*N*-5-hexyonate neamine to the peptoid backbone and **Az** indicates the unconjugated (azide-displaying backbone Figure 2)). **4N-2-DR$_9$** and **4K-2-DR$_9$** have similar cellular permeabilities, while **4Az-2-DR$_9$** is taken up by 75-fold more cells than **4K-2**. It is likely that the decreased cellular permeability of **4N-2-DR$_9$** and **4K-2-DR$_9$** relative to **4Az-2-DR$_9$** is due to the highly cationic aminoglycoside cargo. Confocal microscopy images confirm that **4K-2-DR$_9$** is permeable to almost all cells after longer incubation times (16 h, Figure 5). In all cases, there is no change in the number of cells that are stained by propidium iodide, which indicates cell death, relative to cells that are not treated with compound (Supporting Information Table S-3). Thus, the addition of a **DR$_9$** tag enhances cell uptake by greater than 10-fold while not at the expense of toxicity. Furthermore, the addition of cargo (**K** or **N** modules) onto a peptoid with **DR$_9$** decreases uptake.

In Vitro Potency and Affinity of nK-2-DR$_9$ Compounds.

The potency of the second-generation compounds for disruption of the r(CUG)$_{10}$–MBNL1 complex are summarized in Table 1 (and the Supporting Information). **2K-2-DR$_9$** and **4K-2-DR$_9$** disrupt the r(CUG)$_{10}$–MBNL1 complex *in vitro* with IC$_{50}$s of 1430 ± 160 nM and 240 ± 5 nM, while the corresponding monomer, **FITC-K** has an IC$_{50}$ > 250 μM. Once normalized for the number of **K** units, the multivalent effect[37] for **4K-2-DR$_9$** is >250-fold. Control peptoids in which the backbone in unconjugated (**4Az-2-DR$_9$**) or conjugated to a neamine derivative (**4N-2-DR$_9$**) have IC$_{50}$s of 5400 ± 510 and 1030 ± 90 nM, respectively. Thus, display of the appropriate module, **K**, imparts improved potency (by at least 5-fold) for the disruption of the preformed r(CUG)$_{10}$–MBNL1 complex. The observation that both **4Az-2-DR$_9$** and **4N-2-DR$_9$** inhibit the r(CUG)$_{10}$–MBNL1 complex suggests that the addition of the **DR$_9$** tag causes some level of nonspecific binding of the compounds to RNA, which is not unexpected. This is further verified by the IC$_{50}$ for **4K-2**, which is 16 300 μM in this assay. The large difference in IC$_{50}$ between **4K-2** and **4K-2-DR$_9$** is likely because the **DR$_9$** conjugate occupies a larger amount of the RNA's surface area. A larger difference in potency was previously observed for **4K-2** and **4N-2** (>33-fold) than for **4K-2-DR$_9$** and **4N-2-DR$_9$**, although these experiments were completed using a different assay.[15]

We previously reported that the distance between **K** modules also affects potency and affinity.[15] As shown in Figure 1, the

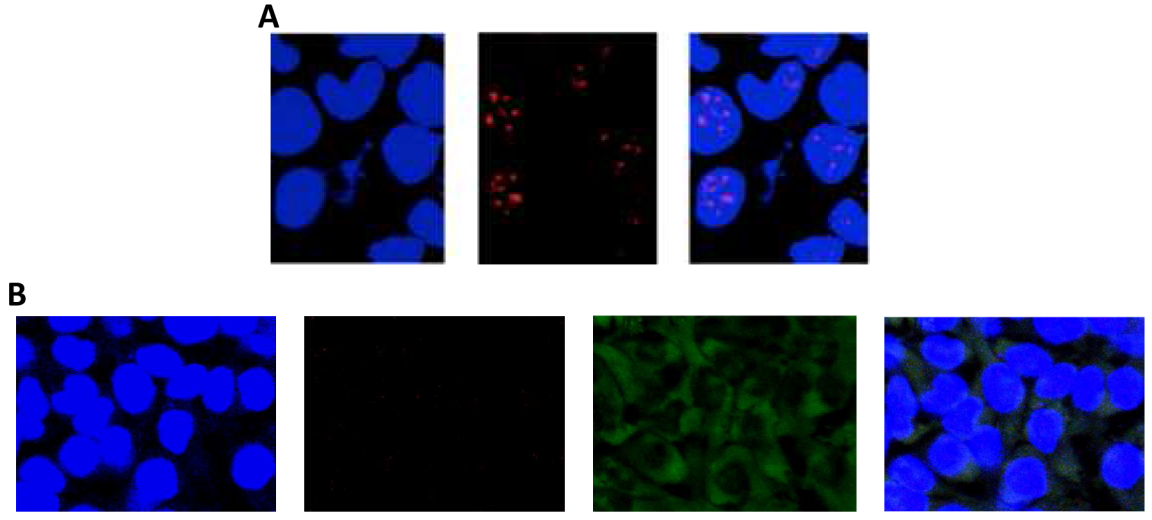

Figure 5. **4K-2-DR$_9$** disrupts the formation of nuclear foci in a DM1 model system as assayed by fluorescence *in situ* hybridization. (A) Confocal microscopy images of untreated cells that express r(CUG)^{exp}. From left to right: DAPI fluorescence (nuclear stain), Cy3 fluorescence (probe for r(CUG)^{exp}), and an overlay of these images. (B) Confocal microscopy images of cells that express r(CUG)^{exp} after treatment with **4K-2-DR$_9$** for 16 h. From right to left: DAPI fluorescence (nuclear stain), Cy3 fluorescence (probe for r(CUG)^{exp}), fluorescein fluorescence (uptake of **4K-2-DR$_9$**), and an overlay of these images. The **4K-2-DR$_9$** compound markedly reduces the number of nuclear foci, as expected, since the compound improves pre-mRNA splicing and translation defects.

dx.doi.org/10.1021/cb3001606 | *ACS Chem. Biol.* 2012, 7, 1984–1993

Table 1. Stoichiometries and Binding Affinities of Small Molecules for RNA and Their Potencies for Inhibition of the r(CUG)$_{10}$−MBNL1 Complex

	r(CUG)$_{12\times2}$		tRNA			
compounds	K_d (nM)	stoichiometry	K_d (nM)	stoichiometry	IC_{50} for r(CUG)$_{10}$−MBNL1 (μM)[a]	M.V.[b]
FITC-K	1000 ± 250[c]	11[c]	>10000	NM	>250	
4K-2	4 ± 1[c]	2.6[c]	>2000	<1:10	16 ± 1	>4
2K-4	NM	NM	NM	NM	170 ± 14	>0.7
3K-4	NM	NM	NM	NM	93 ± 10	>0.9
2K-2-DR$_9$	NM	NM	NM	NM	1.43 ± 0.16	>87
2K-4-DR$_9$	NM	NM	NM	NM	55 ± 0.7	>2
2N-4-DR$_9$	NM	NM	NM	NM	9 ± 1	>13
3K-4-DR$_9$	NM	NM	NM	NM	26 ± 6	>3
4K-2-DR$_9$	3.5 ± 1.8	3.7 ± 1.2	>2000	<1:10	0.240 ± 0.005	>260
4Az-2-DR$_9$	>2000	<1:5	>2000	<1:10	5.4 ± 0.51	>11
4N-2-DR$_9$	>2000	<1:5	>2000	<1:10	1.03 ± 0.09	>60
MBNL1	250[c]		NM	NM	NM	

[a]These experiments were completed by using the qTR-FRET assay described in the Methods section. The r(CUG)$_{10}$−MBNL1 complex was preformed followed by the addition of MBNL1; thus, the IC_{50}s are for displacement. [b]Values for multivalent effects. These values are calculated by normalizing the IC_{50} for the number of RNA-binding modules displayed on a peptoid backbone by the IC_{50} for the **K** module, or **FITC-K**.[15] [c]Data were taken from a previous report.[15]

optimal distance for r(CUG)^{exp} is afforded by two propylamine spacing modules, while the optimal distance for r(CCUG)^{exp} is four propylamines. In order to determine if conjugation of **DR$_9$** affects the optimal distance between **K** modules for r(CUG)^{exp}, the potencies of **2K-4-DR$_9$**, **3K-4-DR$_9$**, and **2N-4-DR$_9$** were determined (Table 1). As expected, **2K-4-DR$_9$** is a 38-fold weaker inhibitor of the r(CUG)−MBNL1 complex (IC_{50} = 55 μM) than **2K-2-DR$_9$**. Increasing the valency to **3K-4-DR$_9$** improves potency by ∼2-fold (26 μM), but it is still a less potent inhibitor by ∼18-fold than **2K-2-DR$_9$** and ∼100-fold weaker inhibitor than **4K-2-DR$_9$**. Interestingly, **2N-4-DR$_9$** is a better inhibitor than **2K-4-DR$_9$** (IC_{50} = 9 μM; ∼6-fold less potent than **2K-2-DR$_9$**), suggesting that the optimal distance between RNA-binding modules is ligand-dependent.

To further understand the nature of inhibition of the complex and the effect of affinity of the RNA−ligand complex, binding measurements were completed with **4K-2-DR$_9$** and the control compounds (Table 1). The RNA used in these studies contains 12 5′CUG/3′GUC motifs or 24 r(CUG) repeats (r(CUG)$_{12\times2}$) embedded in a hairpin cassette.[15] This construct was used so that comparisons could be made to binding affinities reported previously.[15] The data are summarized in Table 1.

The RNA-binding module, **FITC-K**, a fluorescently labeled derivative of 6′-*N*-5-hexynoate kanamycin A has a previously reported K_d of 1 μM.[13] The affinities of the modularly assembled compounds, however, are much higher. For example, **4K-2** has a binding affinity of 4 nM, and **4K-2-DR$_9$** has a K_d of 3.5 nM. **4K-2-DR$_9$** binds to r(CUG)$_{12\times2}$ with a stoichiometry of 3.7 ± 1.2. Since the RNA target contains 12 copies of the 5′CUG/3′GUC motif, the stoichiometry ndicates that each K module approximately interacts with each 5′CUG/3′GUC motif. This was expected based on previous experiments with **4K-2** and other related compounds.[13]

Additionally, **4K-2-DR$_9$** was tested for binding to potential cellular bystander RNA, using bulk yeast tRNA. The compound interacts with tRNAs very weakly with a K_d of greater than 2 μM. The control compounds, **4Az-2-DR$_9$** and **4N-2-DR$_9$**, bind tRNA and r(CUG)$_{12\times2}$ very weakly; binding curves indicate that the K_ds are greater than 2 μM. The addition of the uptake tag does induce some nonspecific RNA binding, as expected and as evidenced by the protein displacement data (Table 1).

Biological Efficacy of nK-2-DR$_9$ Compounds in Cell-Based Model Systems of DM1. Next, the compounds and their appropriate controls were studied for modulating the toxicity of r(CUG)^{exp} in cell-based models of DM1. Three models were used that probe (i) r(CUG)^{exp} toxicity derived from pre-mRNA splicing defects due to sequestration of MBNL1;[19,26] (ii) r(CUG)^{exp} toxicity derived from nuclear retention, and thus reduced translation, of the *DMPK* mRNA;[27,28] and, (iii) formation of nuclear foci due to r(CUG)^{exp}−protein complexes.[29,30]

Improvement of Pre-mRNA Splicing Defects. Pre-mRNA alternative splicing was assayed in HeLa cells as described above.[32] Briefly, cells were transfected with a DM1 mini-gene that expresses 960 interrupted r(CUG) repeats and a pre-mRNA splicing reporter mini-gene of interest.[31,32] We first investigated the effect of the compounds on the alternative splicing of the cTNT mini-gene,[21] the parent gene of which is mis-spliced in DM patients.[21,38,39] In healthy cells, MBNL1 binds upstream of exon 5 in the cTNT pre-mRNA and represses its inclusion.[38,40] In the DM1 model system, approximately 65% of exon 5 is included in cTNT mRNA in the absence of r(CUG)^{exp}, while approximately 90% of exon 5 is included in the presence of r(CUG)^{exp} (Figure 3).

As shown in Figure 3, **2K-2-DR$_9$** and **4K-2-DR$_9$** improve the pre-mRNA splicing defect observed in the cTNT mini-gene toward healthy/wild-type levels (no r(CUG)^{exp} expression) at micromolar concentrations. For **2K-2-DR$_9$**, pre-mRNA splicing defects improve ∼50% when cells are treated with 2 and 20 μM compound (two-tailed p value = 0.0418), while no effect is observed at lower concentrations. For **4K-2-DR$_9$**, pre-mRNA splicing defects are only modestly affected at 1 and 0.1 μM; however, pre-mRNA splicing is restored to levels observed in the absence of r(CUG)^{exp} when cells are treated with 10 μM compound (two-tailed p value = 0.0309). Thus, designed compounds improve pre-mRNA alternative splicing toward a non-DM1-like state to varying extents, with **4K-2-DR$_9$** being more efficacious *in vitro* and *in vivo*.

A series of control experiments were also completed. First, **4Az-2-DR$_9$** and **4N-2-DR$_9$** were also studied for affecting pre-

dx.doi.org/10.1021/cb3001606 | *ACS Chem. Biol.* 2012, 7, 1984−1993

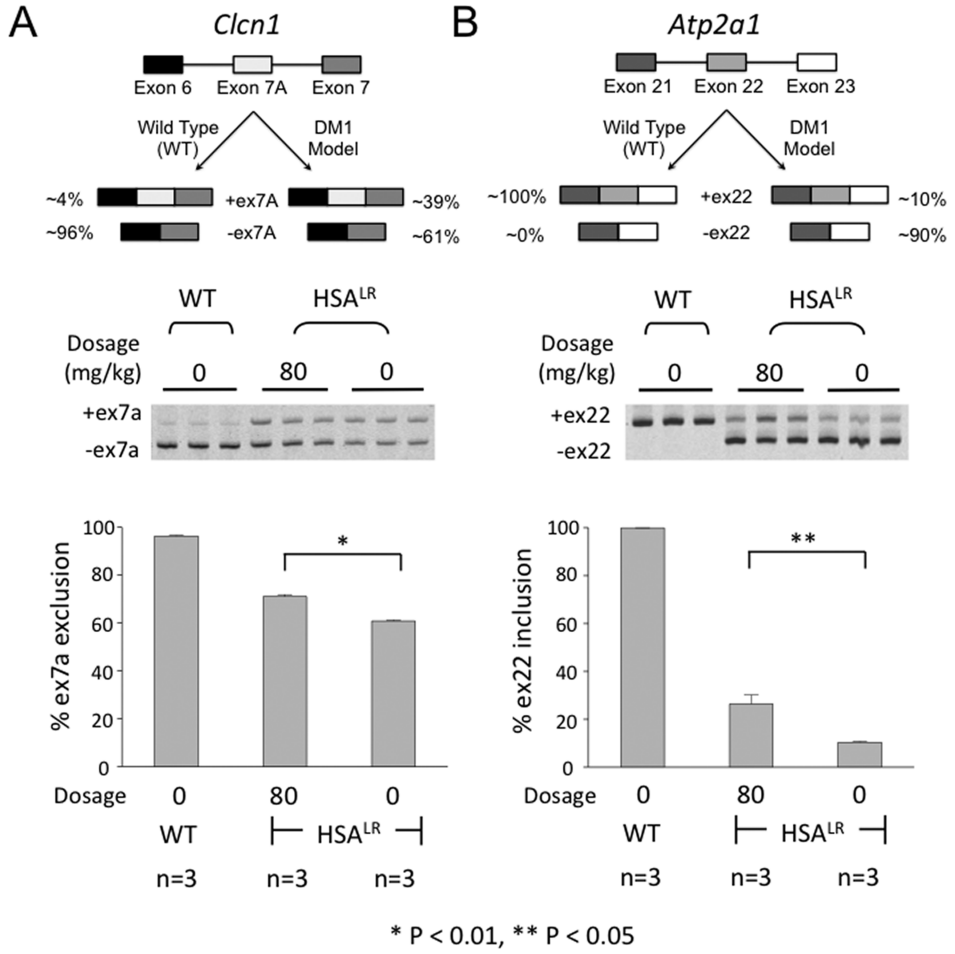

Figure 6. **4K-2-DR$_9$** improves pre-mRNA splicing defects in the muscle-specific chloride ion channel (*Clcn*1) and sarco(endo)plasmic reticulum Ca^{2+} ATPase 1 (*Serca*1/*Atp2a*1) pre-mRNAs in a DM1 mouse model. The DM1 mouse model expresses the human skeletal actin (HSA) transgene containing 250 CTG repeats (HSA^{LR}; where LR indicates long repeats). Wild-type mice (WT) are FVB mice. All dosages are in mg/kg. (A) Top, schematic of *Clcn*1 alternative splicing in wild-type and DM1 mice. Bottom, analysis of *Clcn*1 alternative splicing by RT-PCR when mice are treated with **4K-2-DR$_9$** including a representative gel image and a plot of the corresponding data ($p = 0.0022$). The three lanes under each dosage in the gel image correspond to the results from treatment of three different mice. (B) Top, schematic of *Atp2a*1 alternative splicing in wild-type and DM1 mice. Bottom, analysis of *Atp2a*1 alternative splicing by RT-PCR when mice are treated with **4K-2-DR$_9$** including a representative gel image and a plot of the corresponding data ($p = 0.0491$). The three lanes under each dosage in the gel image correspond to the results from treatment of three different mice.

mRNA splicing. The control compounds were chosen to investigate the role of the RNA-binding module. The compounds are weak *in vitro* inhibitors (Table 1). As shown in Figure 3, neither compound improves cTNT pre-mRNA splicing. Additional control experiments demonstrated that neither **2K-2-DR$_9$** nor **4K-2-DR$_9$** affect (i) the alternative splicing of the cTNT mini-gene in the absence of $r(CUG)^{exp}$ (Figure 3B); (ii) the alternative splicing of a *PLEKHH*2 mini-gene, the alternative splicing of which is not regulated by MBNL1 (Figure 3B); and, (iii) the alternative splicing of endogenous genes (*CAMKK*2 and *TTC*8), which are also not regulated by MBNL1 (data not shown).

Improvement of Translational Defects. In order to determine if **2K-2-DR$_9$** or **4K-2-DR$_9$** can improve DM1-associated translational defects, a stably transfected cell line in which $r(CUG)_{800}$ was placed in the 3′ UTR of firefly luciferase mRNA was employed (Figure 4).[31] As mentioned above, expression of luciferase is low due to the binding of $r(CUG)_{800}$ to MBNL1 and other proteins, resulting in nuclear retention of the luciferase mRNA. In good agreement with the results of the pre-mRNA splicing assays described above, **2K-2-DR$_9$** and **4K-2-DR$_9$** increase the nuclear export and translation of the luciferase mRNA as determined by an increase in luciferase activity. For example, 0.3 and 1.2 μM of each compound stimulates luciferase production by, at best, 20%. However, both compounds stimulate luciferase production by over 50% and by as much as 90% when cells are dosed with 5 or 20 μM compound. In contrast, no effect on luciferase activity was observed when the cells were treated with as much as 20 μM of the two control compounds **4Az-2-DR$_9$** and **4N-2-DR$_9$**.

Control assays were completed in which **2K-2-DR$_9$** and **4K-2-DR$_9$** were tested for nonspecific production of luciferase by using a luciferase mRNA without $r(CUG)^{exp}$ in the 3′ UTR. No change in luciferase production was observed when the cells were treated with as much as 20 μM **2K-2-DR$_9$** or **4K-2-DR$_9$**.

Disruption of Nuclear Foci. Another hallmark of DM1-affected cells is the presence of nuclear foci that consist of $r(CUG)^{exp}$–protein complexes.[26] Therefore, a fluorescence *in situ* hybridization assay (FISH) was used to probe if **4K-2-DR$_9$** can decrease the occurrence of nuclear foci. HeLa cells were transfected with the DM1 mini-gene and treated with **4K-2-DR$_9$**. The cells were then probed with a 2′-*O*-methyl

dx.doi.org/10.1021/cb3001606 | *ACS Chem. Biol.* 2012, 7, 1984–1993

oligonucleotide labeled with Cy3 that is complementary to r(CUG)^{exp}. The cells were then imaged via confocal microscopy (Figure 5). In the absence of **4K-2-DR$_9$**, multiple nuclear foci are observed in each cell, which correspond to r(CUG)^{exp}–protein complexes (Figure 5a). Upon the addition of **4K-2-DR$_9$**, however, there is a marked reduction in the number of the nuclear foci, and the small number of foci that remain are much smaller in size compared to those observed in untreated cells. Since **4K-2-DR$_9$** is labeled with fluorescein, cellular permeability and localization can also be imaged. Fluorescence from the compound is observed in almost every cell and is highly abundant in the cytoplasm with some nuclear localization.

The microscopy data support the results obtained from the luciferase reporter system used to assay the DM1 translational defect. For example, if **4K-2-DR$_9$** was completely localized to the nucleus, then it could cause a further decrease in the production of luciferase by increasing the transcript's nuclear retention. The observation that **4K-2-DR$_9$**, however, enhances luciferase production and is mainly cytoplasmic with some nuclear localization lends some support to a mechanism in which **4K-2-DR$_9$** binding to r(CUG)^{exp} displaces MBNL1 and enables cytoplasmic transport.

4K-2-DR$_9$ Improves pre-mRNA Splicing Defects in a Mouse Model of DM1. A mouse model of DM1 has been reported in which expanded r(CUG) repeat are expressed using a skeletal actin promoter (HSA^{LR}).[20] The presence of the repeats causes the mis-splicing of the muscle-specific chloride ion channel (*Clcn*1) and the sarco(endo)plasmic reticulum Ca^{2+} ATPase 1 (*Serca*1/*Atp*2*a*1) pre-mRNAs.[41−44] Normal adult mice have a *Clcn*1 exon 7a exclusion rate of 96%; DM1 mice have an exclusion rate of 61% (Figure 6). When DM1 mice are dosed with 80 mg/kg of **4K-2-DR$_9$**, the exclusion rate is partially rescued to 71% (Figure 6). These improvements in splicing are statistically significant as determined by a *t* test (p = 0.0022). *Atp*2*a*1 mis-splicing is also partially rescued. In normal adult mice, the inclusion rate for exon 22 is 100%, while the inclusion rate in the HSA^{LR} line is only 10% (Figure 6). When mice are dosed with 80 mg/kg of **4K-2-DR$_9$**, splicing is partially rescued with an inclusion rate of 26% (Figure 6). Again, the improvement in splicing is statistically significant (p = 0.0491).

Comparison to Other Studies. Previous studies have reported three other compounds that improve DM1-associated defects in cell culture. They include pentamidine,[32] *bis*-benzimidazole (**H1**),[45] and modularly assembled compounds displaying a derivative of Hoechst 33258 as the RNA-binding module (**2H-4**, **3H-4**, and **4H-4**).[31] The concentrations required to afford bioactivity is much greater with the lower molecular weight, and thus more drug-like, small molecules (pentamidine and **H1**) than with the modularly assembled structures. For example, the IC$_{50}$s of **H1** and pentamidine that improve pre-mRNA splicing defects are 500 and 50 μM, respectively.[32,45] The modularly assembled compounds **2H-4**, **3H-4**, and **4H-4** restore splicing patterns to levels that are observed in the absence of r(CUG)^{exp} at low micromolar concentrations (10, 50, or 50 μM, respectively).[31] Thus, **2K-2-DR$_9$** and **4K-2-DR$_9$** are as effective in these cell-based assays as other modularly assembled compounds targeting r(CUG)^{exp} and are much more effective than bioactive monomeric ligands.

Improvement of the translational defect was also probed with the modularly assembled Hoechst 33258 compounds.[31] **2H-4**, **3H-4**, and **4H-4** increased translation by 100% at 6, 3, and 3 μM, respectively.[31] **2K-2-DR$_9$** and **4K-2-DR$_9$** also stimulate translation; dosing of 20 μM of either compound increases translation by 80−90%. Thus, **2K-2-DR$_9$** and **4K-2-DR$_9$** are slightly less effective than the **nH-4** compounds that were previously described.

FUTURE DIRECTIONS AND CONCLUSIONS

In this report, we determined that multivalent small molecules that display an aminoglycoside derivative can mitigate the toxicity of r(CUG)^{exp} RNA that causes DM1. By conjugating a cellular uptake tag onto first-generation compounds, the compound has improved cellular permeability and improves DM1-assoicated defects in cell and animal models. Traditionally, most RNA drug targets have been difficult to exploit as targets for small molecules. This and other studies, however, have shown that small molecules that target RNA and modulate its function in both cellular and animal models of disease can be designed.

Further developments in this area will focus on the study of modularly assembled small molecules targeting the r(CCUG)^{exp} that causes DM2;[13,16] it is likely that these compounds will be bioactive upon conjugation to a **DR$_9$** tag. Previous studies have shown that alterations in the spacing submonomer, propylamine in **4K-2**, can affect cell uptake and localization in various cell lines.[33] Thus, there is the possibility that the **DR$_9$** tag may no longer be required for bioactivity. Development in these areas will be reported in due course.

METHODS

Quantitative Time-Resolved Fluorescence Resonance Energy Transfer (qTR-FRET) Assay. The qTR-FRET assay used to determine IC$_{50}$s for inhibition of the r(CUG)$_{10}$–MBNL1 complex is based on a previously published report.[46] Briefly, 5′-biotinylated r(CUG)$_{10}$ was folded in 1× folding buffer (20 mM HEPES, pH 7.5, 110 mM KCl, and 10 mM NaCl) by heating at 60 °C followed by slowly cooling to room temperature on the benchtop. The buffer for r(CUG)$_{10}$ was adjusted to 1× assay buffer (20 mM HEPES, pH 7.5, 110 mM KCl, 10 mM NaCl, 2 mM $MgCl_2$, 2 mM $CaCl_2$, 5 mM DTT, 0.1% BSA, and 0.5% Tween-20), and MBNL1–His$_6$ was added. The final concentrations of RNA and MBNL1 were 80 nM and 60 nM, respectively. The sample was allowed to equilibrate at room temperature for 5 min, and then, the compound of interest was added. After 15 min, strepatividin-XL665 (cisbio Bioassays) and anti-His$_6$-Tb (cisbio Bioassays) were added to final concentrations of 40 nM and 0.44 ng μL^{-1}, respectively, in a total volume of 10 μL. The samples were incubated for 1 h at room temperature and then transferred to a well of a white 384-well plate.

Time-resolved fluorescence was measured on a Molecular Devices SpectraMax M5 plate reader. Fluorescence was first measured using an excitation wavelength of 345 nm and an emission wavelength of 545 nm (fluorescence due to Tb). TR-FRET was then measured by using an excitation wavelength of 345 nm, an emission wavelength of 665 nm, a 200 μs evolution time, and a 1500 μs integration time.

The ratio of fluorescence intensity of 545 and 665 nm as compared to the ratios in the absence of ligand and in the absence of RNA were used to determine IC$_{50}$s. The percentage of MBNL1 binding that was inhibited was plotted versus ligand concentration and the resulting curve was fit to SigmaPlot's 4-parameter logistic function in order to determine the IC$_{50}$ (eq 1):

$$y = D + \frac{A - D}{1 + \left(\frac{x}{IC_{50}}\right)^{\text{hillslope}}} \quad (1)$$

where y is the percentage of MBNL1 bound, D is the minimum response plateau, A is the maximum response plateau, and x is the concentration of ligand. A and D are typically 100% and 0%,

respectively. In cases of weak inhibition, IC_{50}s were determined by fitting the curves to a straight line.

RNA Binding Assays. The affinities of RNA–ligand complexes were determined as previously described[13,15] using a fluorescence emission-based assay. Briefly, RNA was annealed in 1× MBNL buffer (50 mM Tris HCl, pH 8.0, 50 mM NaCl, 50 mM KCl, and 1 mM $MgCl_2$) without $MgCl_2$ by incubating at 60 °C for 5 min followed by slowly cooling to room temperature. Then, $MgCl_2$, BSA, and ligand of interest were added to final concentrations of 1 mM, 40 μg mL^{-1}, and 100 nM, respectively. The RNA was serially diluted in 1× MBNL buffer containing 40 μg mL^{-1} BSA and 100 nM ligand and incubated for 1 h at room temperature. Fluorescence intensity was determined using a BioTek FLX-800 plate reader. Scatchard analyses were completed to determine stoichiometry and dissociation constants, accounting for statistical effects by using a functional form of the Scatchard equation for large ligands binding to a lattice (eq 2):[47,48]

$$\frac{v}{[L]} = \frac{N(1 - lv/N)}{k}\left(\frac{1 - lv/N}{1 - (l-1)v/N}\right)^{l-1} \quad (2)$$

where v is the moles of ligand per moles of RNA lattice, $[L]$ is the concentration of ligand, N is the number of repeating units on the RNA, l is the number of consecutive lattice units occupied by the ligand, and k is the microscopic dissociation constant. This equation simplifies to the commonly used form of the Scatchard equation for simple systems.[47,48] Experiments were completed in triplicate, and the reported errors are the standard deviations in those measurements.

Improvement of Splicing Defects in a Cell Culture Model Using RT-PCR. In order to determine if the compounds improve splicing defects *in vivo*, a previously reported method was employed.[32] Briefly, HeLa cells were grown as monolayers in 96-well plates in growth medium (1× DMEM, 10% FBS, and 1× GlutaMax (Invitrogen)). After the cells reached 90–95% confluency, they were transfected with 200 ng of total plasmid using Lipofectamine 2000 reagent (Invitrogen) per the manufacturer's standard protocol. Equal amounts of a plasmid expressing a DM1 mini-gene with 960 CTG repeats [21] and a mini-gene of interest (cTNT [21] or *PLEKHH2* [40]) were used. Approximately 5 h post-transfection, the transfection cocktail was removed and replaced with growth medium containing the compound of interest. After 16–24 h, the cells were lysed in the well, and total RNA was harvested with a Qiagen RNAEasy kit. An on-column DNA digestion was completed per the manufacturer's recommended protocol.

A sample of RNA was subjected to reverse transcription-polymerase chain reaction (RT-PCR) as previously described,[40] except 5 units of AMV Reverse Transcriptase from Life Sciences were used. Approximately 300 ng were reverse transcribed, and 150 ng were subjected to PCR using a radioactively labeled forward primer. RT-PCR products were observed after 25–30 cycles of 95 °C for 1 min; 55 °C for 1 min; 72 °C for 2 min; and a final extension at 72 °C for 10 min. The products were separated on a denaturing 5% polyacrylamide gel and imaged using a Typhoon phosphorimager.

Control experiments were also completed in which HeLa cells were transfected with a plasmid encoding a mini-gene with five CTG repeats in the 3′ UTR or with a mini-gene that encodes a pre-mRNA whose splicing is not controlled by MBNL1 (*PLEKHH2*[40]). The effect of the compound on the splicing of endogenous mRNAs not regulated by MBNL1 (*TTC8* and *CAMKK2*) was also determined as previously described.[32] Differences in alternative splicing were evaluated by a t test. Please see the Supporting Information for a list of the primers used for each gene.

Disruption of Nuclear Foci Using Fluorescence *In Situ* Hybridization (FISH).[32] HeLa cells were grown as monolayers in Mat-Tak glass-bottomed, 96-well plates. After the cells reached 90–95% confluency, they were transfected with 200 ng of a plasmid encoding a DM1 mini-gene[21] using Lipfoectamine 2000 per the manufacturer's standard protocol. The transfection cocktail was removed 5 h post-transfection, and the compound of interest was added in the growth medium.

After 16–24 h, the cells were washed with 1× DPBS and fixed with 4% paraformaldehyde in 1× DPBS for 10 min at 37 °C/5% CO_2. After washing with 1× DPBS, the cells were permeabilized with 1× DPBS + 0.1% Triton X-100 for 10 min at room temperature. The cells were washed with 1× DPBS + 0.1% Triton X-100 and then with 30% formamide in 2× SSC buffer (30 mM sodium citrate, pH 7.0, and 300 mM NaCl) for 10 min at room temperature.

The cells were incubated in 1× FISH buffer (30% formamide, 2× SSC buffer, 66 μg mL^{-1} bulk yeast tRNA, 2 μg mL^{-1} BSA, 2 mM vanadyl complex (New England Bio Laboratories), and 1 ng μL^{-1} DY547–2′OMe-(CAGCAGCAGCAGCAGC)) for 2 h at 37 °C. They were then washed with 30% formamide in 2× SSC for 30 min at 42 °C, 1× SSC for 30 min at 37 °C, and 1× DPBS + 0.1% Triton X-100 for 5 min at room temperature. Finally, nuclei were stained by incubating the cells with 1 μg mL^{-1} DAPI for 5 min at room temperature. The cells were washed with 1× DPBS + 0.1% Triton X-100, and 100 μL of 1× DPBS were added to each well. The cells were imaged using an Olympus FluoView 1000 Confocal Microscope at 60× magnification.

Treatment in Mice. All experimental procedures, mouse handling, and husbandry were completed in accordance with the Association for Assessment and Accreditation of Laboratory Animal Care. A mouse model for DM1, HSA^{LR} in line 20b,[20] was used to investigate if **4K-2-DR$_9$** improves splicing defects in animals. HSA^{LR} mice express human skeletal actin RNA with r(CUG)^{exp} in the 3′ UTR. Age- and gender-matched HSA^{LR} mice were injected intraperitoneally with 80 mg kg^{-1} **4K-2-DR$_9$** in saline or saline alone once per day for 7 days. Mice were sacrificed one day after the last injection. The vastus muscle was removed, and the RNA was extracted. cDNA was synthesized as previously described.[44] PCR amplification was carried out for 22–24 cycles with the following primer pairs: *Clcn*1 forward, 5′-TGAAGGAATACCTCACACTCAAGG and reverse, 5′-CACGGAA-CACAAAGGCACTG; *Atp2a*1 forward, 5′-GCTCATGGTCCTCAA-GATCTCAC and reverse, 5′-GGGTCAGTGCCTCAGCTTTG. The PCR products were separated by polyacrylamide gel electrophoresis, and the gel was stained with SYBR Green I (Invitrogen). The gel was imaged with a laser fluorimager (Typhoon, GE Healthcare) and the products quantified using ImageQuant. A t test was used to determine the statistical significance of differences between two groups.

■ ASSOCIATED CONTENT

Ⓢ Supporting Information

Methods for the chemical synthesis of **nX-2-DR$_9$** and **nX-4-DR$_9$** compounds; characterization of new compounds including mass spectra and analytical HPLC traces; primers used in RT-PCR analysis; summary of flow cytometry data; representative IC_{50} plots. This material is available free of charge via the Internet at http://pubs.acs.org.

■ AUTHOR INFORMATION

Corresponding Author

*E-mail: Disney@scripps.edu.

Notes

The authors declare no competing financial interest.

■ ACKNOWLEDGMENTS

We thank S. Matosevic for assistance with confocal microscopy and M. Lee for preliminary studies. This work was funded by the National Institutes of Health (3R01GM079235-02S1 and 1R01GM079235-01A2 to M.D.D.; AR049077 and U54NS48843 to C.A.T.), and by The Scripps Research Institute. M.D.D. is a Camille & Henry Dreyfus New Faculty Awardee, a Camille & Henry Dreyfus Teacher-Scholar, and a Research Corporation Cottrell Scholar.

REFERENCES

(1) Poehlsgaard, J., and Douthwaite, S. (2005) The bacterial ribosome as a target for antibiotics. *Nat. Rev. Microbiol. 3*, 870−881.

(2) Thomas, J. R., and Hergenrother, P. J. (2008) Targeting RNA with small molecules. *Chem. Rev. 108*, 1171−1224.

(3) Guan, L., and Disney, M. D. (2012) Recent Advances in Developing Small Molecules Targeting RNA. *ACS Chem. Biol. 7*, 73−86.

(4) Alvarez-Salas, L. M. (2008) Nucleic acids as therapeutic agents. *Curr. Top. Med. Chem. 8*, 1379−1404.

(5) Iorns, E., Lord, C. J., Turner, N., and Ashworth, A. (2007) Utilizing RNA interference to enhance cancer drug discovery. *Nat. Rev. Drug Discovery 6*, 556−568.

(6) Nesterova, M., and Cho-Chung, Y. S. (2004) Killing the messenger: antisense DNA and siRNA. *Curr. Drug Targets 5*, 683−689.

(7) Boggs, R. T., McGraw, K., Condon, T., Flournoy, S., Villiet, P., Bennett, C. F., and Monia, B. P. (1997) Characterization and modulation of immune stimulation by modified oligonucleotides. *Antisense Nucleic Acid Drug Dev. 7*, 461−471.

(8) Farman, C. A., and Kornbrust, D. J. (2003) Oligodeoxynucleotide studies in primates: antisense and immune stimulatory indications. *Toxicol. Pathol. 31* (Suppl.), 119−122.

(9) Childs-Disney, J. L., Wu, M., Pushechnikov, A., Aminova, O., and Disney, M. D. (2007) A small molecule microarray platform to select RNA internal loop−ligand interactions. *ACS Chem. Biol. 2*, 745−754.

(10) Disney, M. D., Labuda, L. P., Paul, D. J., Poplawski, S. G., Pushechnikov, A., Tran, T., Velagapudi, S. P., Wu, M., and Childs-Disney, J. L. (2008) Two-dimensional combinatorial screening identifies specific aminoglycoside-RNA internal loop partners. *J. Am. Chem. Soc. 130*, 11185−11194.

(11) Velagapudi, S. P., Seedhouse, S. J., French, J., and Disney, M. D. (2011) Defining the RNA internal loops preferred by benzimidazole derivatives via 2D combinatorial screening and computational analysis. *J. Am. Chem. Soc. 133*, 10111−10118.

(12) Disney, M. D., and Childs-Disney, J. L. (2007) Using selection to identify and chemical microarray to study the RNA internal loops recognized by 6′-*N*-acylated kanamycin A. *ChemBioChem 8*, 649−656.

(13) Lee, M. M., Pushechnikov, A., and Disney, M. D. (2009) Rational and modular design of potent ligands targeting the RNA that causes myotonic dystrophy 2. *ACS Chem. Biol. 4*, 345−355.

(14) Pushechnikov, A., Lee, M. M., Childs-Disney, J. L., Sobczak, K., French, J. M., Thornton, C. A., and Disney, M. D. (2009) Rational design of ligands targeting triplet repeating transcripts that cause RNA dominant disease: application to myotonic muscular dystrophy type 1 and spinocerebellar ataxia type 3. *J. Am. Chem. Soc. 131*, 9767−9779.

(15) Lee, M. M., Childs-Disney, J. L., Pushechnikov, A., French, J. M., Sobczak, K., Thornton, C. A., and Disney, M. D. (2009) Controlling the specificity of modularly assembled small molecules for RNA via ligand module spacing: targeting the RNAs that cause myotonic muscular dystrophy. *J. Am. Chem. Soc. 131*, 17464−17472.

(16) Disney, M. D., Lee, M. M., Pushechnikov, A., and Childs-Disney, J. L. (2010) The role of flexibility in the rational design of modularly assembled ligands targeting the RNAs that cause the myotonic dystrophies. *ChemBioChem 11*, 375−382.

(17) Liquori, C. L., Ricker, K., Moseley, M. L., Jacobsen, J. F., Kress, W., Naylor, S. L., Day, J. W., and Ranum, L. P. (2001) Myotonic dystrophy type 2 caused by a CCTG expansion in intron 1 of *ZNF9*. *Science 293*, 864−867.

(18) Savkur, R. S., Philips, A. V., Cooper, T. A., Dalton, J. C., Moseley, M. L., Ranum, L. P., and Day, J. W. (2004) Insulin receptor splicing alteration in myotonic dystrophy type 2. *Am. J. Hum. Genet. 74*, 1309−1313.

(19) Faustino, N. A., and Cooper, T. A. (2003) Pre-mRNA splicing and human disease. *Genes Dev. 17*, 419−437.

(20) Mankodi, A., Logigian, E., Callahan, L., McClain, C., White, R., Henderson, D., Krym, M., and Thornton, C. A. (2000) Myotonic dystrophy in transgenic mice expressing an expanded CUG repeat. *Science 289*, 1769−1773.

(21) Philips, A. V., Timchenko, L. T., and Cooper, T. A. (1998) Disruption of splicing regulated by a CUG-binding protein in myotonic dystrophy. *Science 280*, 737−741.

(22) Goun, E. A., Shinde, R., Dehnert, K. W., Adams-Bond, A., Wender, P. A., Contag, C. H., and Franc, B. L. (2006) Intracellular cargo delivery by an octaarginine transporter adapted to target prostate cancer cells through cell surface protease activation. *Bioconjugate Chem. 17*, 787−796.

(23) Goun, E. A., Pillow, T. H., Jones, L. R., Rothbard, J. B., and Wender, P. A. (2006) Molecular transporters: synthesis of oligoguanidinium transporters and their application to drug delivery and real-time imaging. *ChemBioChem 7*, 1497−1515.

(24) Luedtke, N. W., Carmichael, P., and Tor, Y. (2003) Cellular uptake of aminoglycosides, guanidinoglycosides, and poly-arginine. *J. Am. Chem. Soc. 125*, 12374−12375.

(25) Frankel, A. D., and Pabo, C. O. (1988) Cellular uptake of the tat protein from human immunodeficiency virus. *Cell 55*, 1189−1193.

(26) Cardani, R., Mancinelli, E., Rotondo, G., Sansone, V., and Meola, G. (2006) Muscleblind-like protein 1 nuclear sequestration is a molecular pathology marker of DM1 and DM2. *Eur. J. Histochem. 50*, 177−182.

(27) Mastroyiannopoulos, N. P., Feldman, M. L., Uney, J. B., Mahadevan, M. S., and Phylactou, L. A. (2005) Woodchuck post-transcriptional element induces nuclear export of myotonic dystrophy 3′ untranslated region transcripts. *EMBO Rep. 6*, 458−463.

(28) Amack, J. D., Paguio, A. P., and Mahadevan, M. S. (1999) Cis and trans effects of the myotonic dystrophy (DM) mutation in a cell culture model. *Hum. Mol. Genet. 8*, 1975−1984.

(29) Jiang, H., Mankodi, A., Swanson, M. S., Moxley, R. T., and Thornton, C. A. (2004) Myotonic dystrophy type 1 is associated with nuclear foci of mutant RNA, sequestration of muscleblind proteins and deregulated alternative splicing in neurons. *Hum. Mol. Genet. 13*, 3079−3088.

(30) Wojciechowska, M., and Krzyzosiak, W. J. (2011) Cellular toxicity of expanded RNA repeats: focus on RNA foci. *Hum. Mol. Genet. 20*, 3811−3821.

(31) Childs-Disney, J. L., Hoskins, J., Rzuczek, S., Thornton, C., and Disney, M. D. (2012) Rationally designed small molecules targeting the RNA that causes myotonic dystrophy type 1 are potently bioactive. *ACS Chem. Biol. 7*, 856−862.

(32) Warf, M. B., Nakamori, M., Matthys, C. M., Thornton, C. A., and Berglund, J. A. (2009) Pentamidine reverses the splicing defects associated with myotonic dystrophy. *Proc. Natl. Acad. Sci. U.S.A. 106*, 18551−18556.

(33) Lee, M. M., French, J. M., and Disney, M. D. (2011) Influencing uptake and localization of aminoglycoside-functionalized peptoids. *Mol. BioSyst. 7*, 2441−2451.

(34) Koepsell, H., Lips, K., and Volk, C. (2007) Polyspecific organic cation transporters: structure, function, physiological roles, and biopharmaceutical implications. *Pharm. Res. 24*, 1227−1251.

(35) Fuchs, S. M., and Raines, R. T. (2004) Pathway for polyarginine entry into mammalian cells. *Biochemistry 43*, 2438−2444.

(36) Iozzo, R. V. (1998) Matrix proteoglycans: from molecular design to cellular function. *Annu. Rev. Biochem. 67*, 609−652.

(37) Mammen, M., Choi, S. K., and Whitesides, G. M. (1998) Polyvalent interactions in biological systems: Implications for design and use of multivalent ligands and inhibitors. *Angew. Chem., Int. Ed. 37*, 2755−2794.

(38) Ho, T. H., Charlet, B. N., Poulos, M. G., Singh, G., Swanson, M. S., and Cooper, T. A. (2004) Muscleblind proteins regulate alternative splicing. *EMBO J. 23*, 3103−3112.

(39) Nezu, Y., Kino, Y., Sasagawa, N., Nishino, I., and Ishiura, S. (2007) Expression of *MBNL* and *CELF* mRNA transcripts in muscles with myotonic dystrophy. *Neuromuscul. Disord. 17*, 306−312.

(40) Warf, M. B., and Berglund, J. A. (2007) MBNL binds similar RNA structures in the CUG repeats of myotonic dystrophy and its pre-mRNA substrate cardiac troponin T. *RNA 13*, 2238−2251.

(41) Mankodi, A., Takahashi, M. P., Jiang, H., Beck, C. L., Bowers, W. J., Moxley, R. T., Cannon, S. C., and Thornton, C. A. (2002)

Expanded CUG repeats trigger aberrant splicing of *ClC-1* chloride channel pre-mRNA and hyperexcitability of skeletal muscle in myotonic dystrophy. *Mol. Cell 10*, 35−44.
(42) Charlet, B. N., Savkur, R. S., Singh, G., Philips, A. V., Grice, E. A., and Cooper, T. A. (2002) Loss of the muscle-specific chloride channel in type 1 myotonic dystrophy due to misregulated alternative splicing. *Mol. Cell 10*, 45−53.
(43) Kimura, T., Nakamori, M., Lueck, J. D., Pouliquin, P., Aoike, F., Fujimura, H., Dirksen, R. T., Takahashi, M. P., Dulhunty, A. F., and Sakoda, S. (2005) Altered mRNA splicing of the skeletal muscle ryanodine receptor and sarcoplasmic/endoplasmic reticulum Ca^{2+}-ATPase in myotonic dystrophy type 1. *Hum. Mol. Genet. 14*, 2189−2200.
(44) Lin, X., Miller, J. W., Mankodi, A., Kanadia, R. N., Yuan, Y., Moxley, R. T., Swanson, M. S., and Thornton, C. A. (2006) Failure of MBNL1-dependent post-natal splicing transitions in myotonic dystrophy. *Hum. Mol. Genet. 15*, 2087−2097.
(45) Parkesh, R., Childs-Disney, J. L., Nakamori, M., Kumar, A., Wang, E., Wang, T., Hoskins, J., Housman, D. E., Thornton, C. A., Disney, M. D., and Tran, T. (2012) Design of a bioactive small molecule that targets the myotonic dystrophy type 1 RNA via an RNA motif-ligand database & chemical similarity searching. *J. Am. Chem. Soc. 134*, 4731−4742.
(46) Chen, C. Z., Sobczak, K., Hoskins, J., Southall, N., Marugan, J. J., Zheng, W., Thornton, C. A., and Austin, C. P. (2012) Two high-throughput screening assays for aberrant RNA-protein interactions in myotonic dystrophy type 1. *Anal. Bioanal. Chem. 402*, 1889−1898.
(47) Cantor, C. R., Schimmel, P. R. (1980) *Biophysical Chemistry*, W.H. Freeman and Company, San Francisco.
(48) McGhee, J. D., and Hippel, P. H. V. (1974) Theoretical aspects of DNA−protein interactions: cooperative and non-cooperative binding of large ligands to a one-dimensional homogeneous lattice. *J. Mol. Biol. 86*, 469−489.